

## Melting in super-earth

Lars Stixrude

*Phil. Trans. R. Soc. A* 2014 **372**, 20130076, published 24 March 2014

---

### References

**This article cites 80 articles, 15 of which can be accessed free**  
<http://rsta.royalsocietypublishing.org/content/372/2014/20130076.full.html#ref-list-1>

### Email alerting service

Receive free email alerts when new articles cite this article - sign up in the box at the top right-hand corner of the article or click [here](#)

[rsta.royalsocietypublishing.org](http://rsta.royalsocietypublishing.org)

## Research



CrossMark  
click for updates

**Cite this article:** Stixrude L. 2014 Melting in super-earths. *Phil. Trans. R. Soc. A* **372**: 20130076.

<http://dx.doi.org/10.1098/rsta.2013.0076>

One contribution of 17 to a Theo Murphy Meeting Issue 'Characterizing exoplanets: detection, formation, interiors, atmospheres and habitability'.

### Subject Areas:

extrasolar planets

### Keywords:

interiors, evolution, structure, material properties

### Author for correspondence:

Lars Stixrude

e-mail: [l.stixrude@ucl.ac.uk](mailto:l.stixrude@ucl.ac.uk)

# Melting in super-earths

Lars Stixrude

Department of Earth Sciences, University College London, Gower St, London WC1E 6BT, UK

We examine the possible extent of melting in rock-iron super-earths, focusing on those in the habitable zone. We consider the energetics of accretion and core formation, the timescale of cooling and its dependence on viscosity and partial melting, thermal regulation via the temperature dependence of viscosity, and the melting curves of rock and iron components at the ultra-high pressures characteristic of super-earths. We find that the efficiency of kinetic energy deposition during accretion increases with planetary mass; considering the likely role of giant impacts and core formation, we find that super-earths probably complete their accretionary phase in an entirely molten state. Considerations of thermal regulation lead us to propose model temperature profiles of super-earths that are controlled by silicate melting. We estimate melting curves of iron and rock components up to the extreme pressures characteristic of super-earth interiors based on existing experimental and *ab initio* results and scaling laws. We construct super-earth thermal models by solving the equations of mass conservation and hydrostatic equilibrium, together with equations of state of rock and iron components. We set the potential temperature at the core–mantle boundary and at the surface to the local silicate melting temperature. We find that ancient (~4 Gyr) super-earths may be partially molten at the top and bottom of their mantles, and that mantle convection is sufficiently vigorous to sustain dynamo action over the whole range of super-earth masses.

## 1. Introduction

Melting is a fundamentally important planetary process in our Solar System and is likely to be also important in super-earth exoplanets. The significance of melting is generic because it derives from fundamental properties of liquids generated by partial melting, especially their viscosity and density, which differ significantly from that of coexisting solids. Buoyant transport of liquids is an important source of mass and heat transport even at

low melt fractions, because liquids are so much more mobile owing to their much lower viscosity. At high melt fractions, such as in iron-rich cores and early magma oceans, the characteristic velocities of flow are orders of magnitude larger than in the solid state, allowing for high surface heat flux and for the generation of magnetic fields. The chemical composition of partial melts also differs significantly from coexisting solids: partial melting is an important source of chemical differentiation, such as the production of lower density crust from the mantle, and the freezing out of higher density solids in cooling iron-rich cores.

Our focus here is on those exoplanets that are similar in composition to the terrestrial planets of our solar system, that is dominated by iron and rock components, and which are Earth-sized or larger. Such bodies are likely to be abundant as indicated by an analysis of the composition of stars that host exoplanets, which show heavy element fractions rich in Fe, O, Mg and Si, and with elemental ratios similar to those of Solar System rocky bodies [1]. Mass–radius relationships already show several transiting exoplanets that are consistent with rock–iron compositions, despite observational biases against detection of such relatively small bodies [2–9]. Most transiting exoplanets discovered to date in the super-earth mass range ( $1\text{--}10 M_{\text{E}}$ ) have much larger radii, indicating the presence of large gaseous or icy envelopes. Very recently, super-earth-sized exoplanets have been found within the habitable zone of their host star [10,11].

How hot are the interiors of rocky super-earth exoplanets? The interior temperature controls long-term planetary evolution and processes with potentially observable consequences such as volcanism and magnetic field generation. The volcanic flux and magnetic field strength both scale with the heat flux out of the interior  $F$  [12,13]. Assuming the flux is dominated by thermal convection and neglecting internal heat sources such as those owing to radioactive decay or tidal heating

$$F \propto \left( \frac{\rho^2 \alpha g C_p k^2}{\eta} \right)_{\text{TBL}}^{1/3} (\Delta T_{\text{TBL}})^{4/3}, \quad (1.1)$$

where  $\Delta T_{\text{TBL}}$  is the temperature contrast across the thermal boundary layer, and the properties within the boundary layer:  $\rho$  is density,  $\alpha$  is the volumetric thermal expansivity,  $g$  is gravitational acceleration,  $C_p$  is isobaric heat capacity,  $k$  is thermal conductivity and  $\eta$  is dynamic viscosity [14]. The dependence on planetary mass is weak, and appears explicitly through  $g \propto M_p^{1-2\beta}$ , where  $\beta$  is the exponent of the mass–radius relationship for super-earths ( $\beta \approx 0.27$ ) [15]. We consider two thermal boundary layers: at the surface of the planet,  $\Delta T_{\text{TBL}} = T_p - T_s$ , where  $T_p$  is the interior potential temperature of the mantle, and  $T_s$  is the surface temperature and at the core–mantle boundary  $\Delta T_{\text{TBL}} = T_c - T_{pc}$ , where  $T_c$  is the temperature at the core–mantle boundary and  $T_{pc}$  is the temperature of the adiabat with potential temperature  $T_p$  at the core–mantle boundary.

If the heat flux out of the interior is much less than the stellar flux, then the surface temperature  $T_s$  is controlled by thermal equilibrium with stellar irradiation. In the absence of a thick atmosphere

$$T_s = T_{\star} \sqrt{\frac{R_{\star}}{a}} \left( \frac{1-A}{d} \right)^{1/4}, \quad (1.2)$$

where  $a$  is the orbital radius,  $T_{\star}$  and  $R_{\star}$  are the stellar effective temperature and radius,  $A$  is the Bond albedo and  $d$  is a distribution coefficient:  $d = 4$  in the case of efficient redistribution of stellar irradiation over the whole planetary surface and  $d = 2$  in case the dayside retains all the heat. Observations of thermal emission from 55 Cnc e indicate inefficient redistribution  $d \approx 2$  and a small Bond albedo  $A < 0.5$  [16]. The calculated surface temperatures of transiting super-earth exoplanets discovered so far are very hot compared with those of Solar System planets. In some cases (Kepler-10b, Cnc 55 e, CoRot-7b), the calculated surface temperature ( $d = 4$ ) exceeds the silicate solidus, so that these planets may have molten rock at the surface.

Planets that are molten at the surface likely possess a magma ocean that extends to hundreds of kilometres depth into the planet. Comparison of the silicate melting curve with the silicate adiabat [17] shows that for  $T_s = 2100$  K, similar to that of Kepler-10b assuming  $d = 4$ , the adiabat lies above the liquidus (complete melting) to a pressure  $P = 30$  GPa, and lies between liquidus

and solidus (partial melting) to a pressure  $P > 150$  GPa. These pressures correspond to depths of 400 km for complete melting and greater than 1500 km for partial melting in the case  $M_p = 5 M_\oplus$ . The maximum thickness of the partially molten zone is uncertain, because our knowledge of the silicate melting curve at pressure  $P > 150$  GPa is limited, and because it may depend on the efficiency of interior heat transport between day and nightside, particularly for planets such as Kepler-10b that are very close to their parent star and may be tidally locked [18]. Thick magma oceans may distort the stellar magnetic field because of the relatively high conductivity of silicate melt when compared with solid silicates, similar to the case of the distortion of Jupiter's magnetic field by Io [19]. The electrical conductivity of silicate melts increases with increasing pressure, so that very deep magma oceans may generate their own magnetic field through dynamo action [20].

Planets in the habitable zone are likely to have interior temperatures that greatly exceed their surface temperatures. The reason is that a large fraction of planetary heat is likely left over from the accretion process. The kinetic energy of accretion converted to heat is sufficient to melt a super-earth several times over. However, much of this kinetic energy is rapidly lost during the accretion process via radiation, and only some fraction is deposited in the interior during the planet's formation [21]. The recognition that giant impacts are a generic part of rocky planet accretion has changed our views of this energy balance. Giant impacts are very efficient at depositing heat in the interior, much more so than the infinitesimal accretion that dominated early thinking about this problem.

The importance of impactor size in the deposition of accretional kinetic energy can be illustrated through the following analysis. A hydrodynamical modelling study [22] found that the amount of melt  $M_{\text{melt}}$  produced scales with the kinetic energy of the impactor of mass  $M_i$  and velocity  $v_i$  as

$$E_M M_{\text{melt}} \approx \frac{1}{5} \left( \frac{1}{2} M_i v_i^2 \right), \quad (1.3)$$

where  $E_M$  is the energy required to heat the material from 300 K to above the liquidus, including the latent heat of melting. We have approximated the best-fit computed relationship by equating mass scaling to volume scaling and to one of pure kinetic energy scaling, which is consistent, within uncertainty, to best fit parameters determined by Pierazzo *et al.* [22]. If we take the limit that the deposited heat is efficiently redistributed through the entire planet, and equate the right-hand side of equation (1.3) with the resulting thermal energy:  $M_p C'_p (T_p - T_s)$  then assuming that the entire planet starts off isothermally at  $T_s$ ,

$$T_p = \frac{h'}{C'_p} \left( \frac{1}{2} v_i^2 \right) + T_s, \quad (1.4)$$

where the prime on the heat capacity indicates an effective value that accounts for the latent heat of melting [23], and the efficiency of kinetic energy deposition

$$h' = \frac{1}{5} \frac{M_i}{M_p}. \quad (1.5)$$

We have added a prime to the efficiency factor to distinguish it from the older definition, which relates the kinetic energy to heat deposited only in the impact zone and which was assumed to be independent of impactor mass [21]. This analysis shows that the efficiency of kinetic energy deposition increases with increasing impactor size: giant impacts deposit more heat energy density than smaller impacts.

To examine impact melting in more detail, we have reproduced the analysis of [24] and applied it to super-earths (figure 1). Following that study, we assume that the impact produces a subsurface isobaric core in the form of an internal tangent sphere with radius equal to that of the impactor and pressure and temperature determined by the Hugoniot relation and the impact velocity. Also following Tonks and Melosh, we use dunite as a convenient analogue material

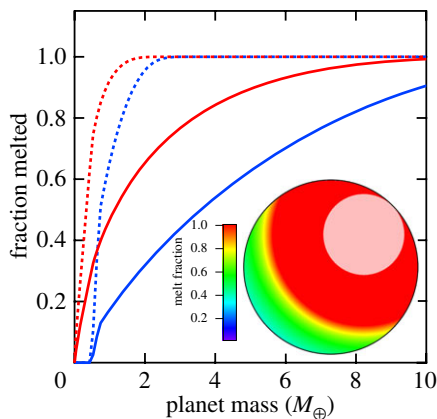


**Figure 1.** Fraction of planetary mass melted by impacts with  $M_i/M_p = 0.1$  (solid lines) and  $M_i/M_p = 0.4$  (dashed lines) and for initial temperatures  $T_0 = 300$  K (blue) and  $T_0 = T_{\text{sol}}$  (red) as a function of planetary mass assuming the minimal impact velocity  $v_i = 11.2 \text{ km s}^{-1} (M_p/M_{\oplus})^{(1-\beta)/2}$ . The inset shows the distribution of melt fraction throughout the planet for  $M_p = 5M_{\oplus}$ ,  $M_i/M_p = 0.1$ , and  $T_0 = T_{\text{sol}}$ . The pink circle represents the completely molten isobaric core. (Online version in colour.)

for the rocky component of super-earths because its Hugoniot is well characterized and widely studied. The impact velocity required to completely melt the isobaric core is small compared with typical impact velocities in the late stages of planetary accretion: for dunite, the critical velocity is  $8.6 \text{ km s}^{-1}$  (Hugoniot pressure  $P_H = 150 \text{ GPa}$ ), equivalent to the escape velocity (and therefore minimum impact velocity) for a planet with mass of only  $0.5 M_{\oplus}$ . Outside the isobaric core, the particle velocity decreases as  $r^{-2}$ , where  $r$  is the distance from the edge of the core, producing concentric spheres of diminishing heating. The completely molten zone can be much larger than the impactor for typical impact velocities. Outside the completely molten zone are concentric spheres of partial melting; the critical velocity for partial melting in dunite is  $6.5 \text{ km s}^{-1}$  ( $P_H = 102 \text{ GPa}$ ). For large amounts of melting geometric corrections become important: one must find the overlapping volume of the melt sphere and the planetary sphere [25].

Results show that substantial melting is expected during the accretion of rocky planets. For example for  $M_p = 5 M_{\oplus}$ ,  $M_i = 0.1 M_p$ , and minimal impact velocity, 60% of the planet is molten if the initial temperature  $T_0 = 300 \text{ K}$ . If we consider the cumulative effect of several impacts during the accretion process, such a cold initial temperature may be unrealistic. If the planet had been completely or substantially molten by a prior impact, we may expect it to cool rapidly, until it approaches the solidus temperature,  $T_{\text{sol}}$  where the viscosity, and the cooling timescale increase rapidly. If we assume that  $T_0 = T_{\text{sol}}$ , then 90% is melted by the impact. Simulations of planetary accretion find that impactors with  $M_i = 0.1 M_p$  are common, and that even larger impacts also occur: perhaps 20% with  $M_i > 0.4 M_p$  [26]. With  $M_i = 0.4 M_p$  and minimal impact velocity, the planet is more than 90% molten for  $M_p > 1.7 M_{\oplus}$  from a cold start and for  $M_p > 0.9 M_{\oplus}$  for  $T_0 = T_{\text{sol}}$ . We have focused on minimal impact velocities in order to obtain conservative estimates of melting and because the probability of accretion, as opposed to impact erosion or hit-and-run events, increases with decreasing impact velocity. In general, the impact velocity  $v_i^2 = 2GM_p/R_p + v_{\infty}^2$ , where  $v_{\infty}$  is the relative velocity at infinite separation, and  $G$  is the gravitational constant. For typical values found in accretion simulations  $v_{\infty} \approx 5 \text{ km s}^{-1}$  [26], the amount of melting for the case with  $M_p = 5 M_{\oplus}$ ,  $M_i = 0.1 M_p$  and  $T_0 = 300 \text{ K}$ , increases by a few per cent. Beyond the scope of the present analysis are factors not considered by Tonks & Melosh [24] that should be considered in future studies of giant impact melting, including the effect of increasing hydrostatic pressure with depth in the target body [27], and the effects of vapourization [28].

Many super-earths may be completely molten at the end of accretion. In addition to the accumulation of kinetic energy derived from one or more giant impacts, the energy released by

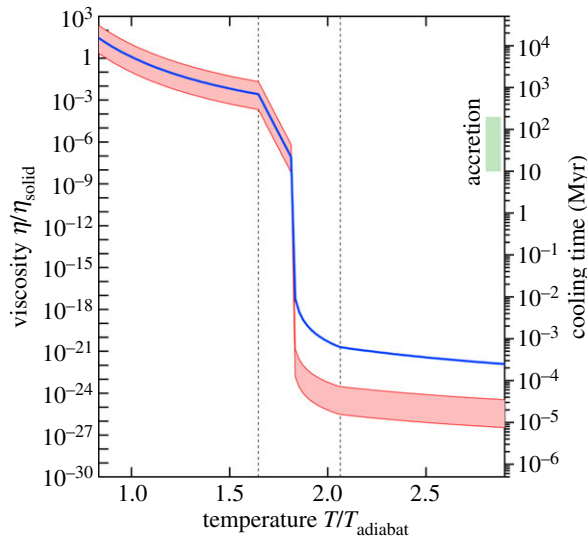


**Figure 2.** Viscosity as a function of temperature at a typical pressure for planetary mantles ( $P = 100$  GPa; red envelope), and cooling time (blue curve, right-hand axis) as a function of temperature. The viscosity and its temperature dependence in the solid state [34], and liquid state [35] are taken from *ab initio* studies. Melt fraction is assumed to vary linearly with temperature between solidus and liquidus, and the dependence of viscosity on melt fraction is taken from experiment [36,37]. The isentropic temperature (2400 K) is computed with HeFESTo assuming a potential temperature of 1600 K [38]; the solidus (3950 K) and liquidus (4950 K) temperatures are from an experimental study [39]. The cooling time is computed from equation (1.7) up to the temperature of the viscosity collapse, and from the scaling appropriate for hard turbulence and an overlying thick atmosphere at higher temperature [35]. The green box indicates typical times of rocky planet accretion [40,41]. (Online version in colour.)

core formation is sufficient in itself to melt the entire planet. The gravitational energy released by core formation is equivalent to a temperature increase of the entire planet [29]

$$T_p - T_s = 2300 \text{ K} \left( \frac{M_p}{M_\oplus} \right)^{1-\beta}, \quad (1.6)$$

where we have assumed that the ratios of mantle to core density, mass and radius are the same as in the Earth, and we have not accounted for the latent heat of melting. For  $M_p = 5 M_\oplus$ , the temperature rise is 7000, or 3500 K if we account for the latent heat of melting. In detail, the energy released by core formation is not distributed uniformly: a large fraction of energy is partitioned into the sinking iron-rich material. In this scenario, the planet at the end of accretion has a superheated core [30]. Cores form easily even in bodies as small as the Moon or Mars before the onset of silicate melting via diapiric instability of the denser iron-rich material [31]. Geochemical evidence indicates that even in bodies as small as asteroids, core formation is a rapid process (few myr) in this case assisted by the energy released by short-lived radioisotopes such as  $^{26}\text{Al}$  [32,33].

How does an initially molten planetary mantle cool? The initial stages of cooling are rapid, with cooling times of only 10 kyr (figure 2). Rapid cooling continues until a significant proportion of the planet has crystallized. The viscosity rises rapidly as the solidus is approached and the cooling time rapidly increases beyond 1 Gyr. The cooling time  $\tau = M_p C_p (T_p - T_s) / 4\pi R_p^2 F$ . For melt-fraction  $\phi \lesssim 0.4$ , and ignoring the variation of the flux with  $g$  and material properties other than the viscosity

$$\tau = 3.9 \text{ Gyr} \left( \frac{M_p}{M_\oplus} \right)^{1-2\beta} \left( \frac{\eta_0(P, T) e^{-\alpha\phi}}{1 \times 10^{21} \text{ Pa s}} \right)^{1/3} \left( \frac{T_p - T_s}{1300 \text{ K}} \right)^{-1/3}, \quad (1.7)$$

where  $\eta_0$  is the melt-free viscosity,  $\phi$  is the melt fraction,  $\alpha \approx 26$  [36] is the melt-fraction exponent, and we have scaled the cooling time to present-day Earth-like values of the heat flux [42], viscosity [43] and the temperature difference [44]. Planets therefore retain most of the heat that is deposited in their interiors since their formation: larger planets retain their heat longer than smaller planets. The retention of heat in the core is still more efficient, because convection cannot penetrate the core–mantle boundary. The distribution of melt fraction in a cooling planet is unlikely to be homogeneous at any stage once crystallization begins, significantly complicating the analysis of the cooling time. For example, it has been proposed that deep melt layers may survive for billions of years protected by an overlying insulating solid layer [45].

The cooling time depends on temperature, and strongly for temperature in between the solidus and liquidus (figure 2). For example, with  $\phi = 0.1$ , the cooling time is half the melt-free value assuming all other values to be equal. This strong dependence suggests a thermal-regulation (homeostatic) mechanism in the evolution of super-earths: as the planet cools towards the solidus, the heat flux diminishes, allowing heat from internal sources to accumulate, warming the planet again. This type of thermal regulation mechanism has been proposed to operate in the terrestrial planets, although the argument did not consider super-solidus temperatures or include the possible influence of partial melt, emphasizing instead the weaker temperature dependence of the melt-free viscosity [46]. A recent study argued for the importance of thermal self-regulation in super-earths [47]. As the planet cools, the viscosity rises, particularly in the deep mantle because of the strong pressure dependence of viscosity, which tends to make convection more sluggish [47,48]. Dynamical simulations show that the planet never cools sufficiently to become so viscous that it stops convecting, because of internal heat generation [47]. The possible effects of partial melting were not considered in these calculations, in part because the large change in viscosity on partial melting poses numerical challenges that are yet to be overcome.

We argue that the thermal state of super-earth interiors in the habitable zone is governed by silicate melting. Partial melt in evolved super-earths, if it exists, is likely to be concentrated in thermal boundary layers. The reason being that in thermal boundary layers, the temperature rises much more steeply than the silicate melting temperature with increasing depth, whereas in the adiabatic, convecting interior, the temperature rises much more slowly than the melting curve. Boundary layer temperatures near the solidus are likely because (i) super-earths start out super-liquidus and cool rapidly until the boundary layer temperature approaches the solidus temperature (figure 2), (ii) cooling becomes inefficient as the solidus is approached, and (iii) heat flux depends strongly on temperature via the boundary layer viscosity, so that thermal regulation is likely to keep the boundary layer temperature nearly constant. A recent study also arrived at the conclusion that the steady-state core–mantle boundary temperature in super-earths is equal to that of silicate melting, albeit using a somewhat different argument [13]. In the present-day Earth, melting is known to occur towards the base of the upper thermal boundary layer, and evidence from seismology indicates anomalous structures in the bottom-most mantle that may be explained by partial melt at the core–mantle boundary [49,50].

Estimates of the melting temperature of major planet forming materials are important for understanding super-earth thermal evolution (figure 3). Our knowledge is still limited, because typical pressures exceed those that can be routinely reached in the laboratory, and *ab initio* simulations have only begun to explore the relevant pressure–temperature regime. For the silicate melting point, we assume the Lindemann melting law [58]

$$T_{\text{Lindemann}} = f^2 \frac{\bar{m} k_B \bar{v}^{2/3} \theta^2}{9\hbar^2}, \quad (1.8)$$

where  $\bar{m}$  and  $\bar{v}$  are the mean atomic mass and volume, respectively,  $k_B$  is the Boltzmann constant,  $\hbar$  is the Planck constant divided by  $2\pi$ ,  $\theta$  is the Debye temperature and  $f$  is the critical ratio of vibration amplitude to atomic spacing at melting. For applications to the core–mantle boundary of super-earths, we assume that the solid phase is  $\text{MgSiO}_3$  post-perovskite [59,60], and compute the volume and Debye temperature as a function of pressure along the 1600 K adiabat from the thermodynamic model of [38]. We chose the value of  $f = 0.137$ , so that the computed melting

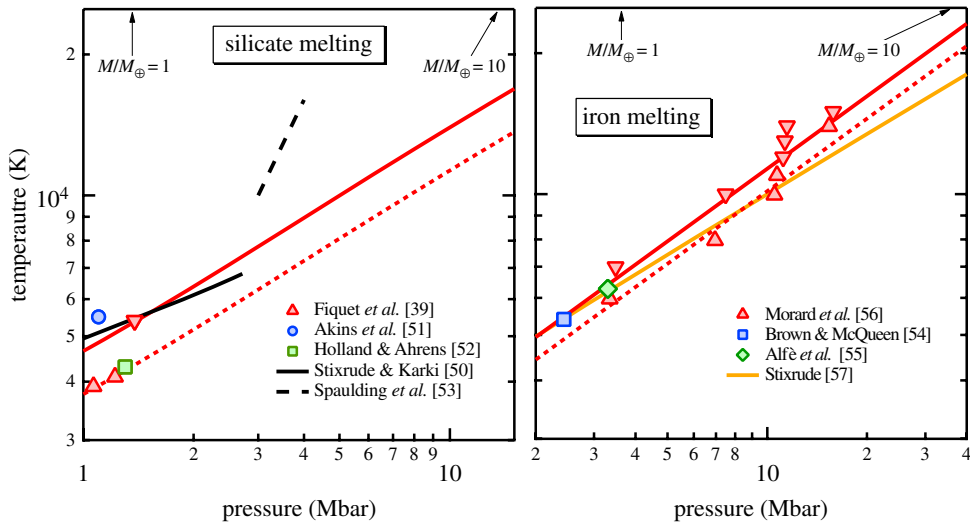


**Figure 3.** Estimates of the melting temperature of silicates (*a*) and iron alloy (*b*) for the pure substance (solid red lines) and accounting for impurities (dashed red lines). Compared with (*a*) experimental measurements of the liquidus [39,51], the solidus [39,52], a proposed superliquidus liquid–liquid phase transition [53], and the *ab initio* melting curve of  $\text{MgSiO}_3$  in the lower pressure perovskite phase [50], and (*b*) determinations of pure iron melting from experiment [54] and *ab initio* theory [55], brackets on the melting curve from *ab initio* theory [56] and the Lindemann law result based on subsolidus *ab initio* phonon calculations [57]. Arrows at the top indicate the pressure at the core–mantle boundary (*a*) and at the planetary centre (*b*). (Online version in colour.)

curve intersects the  $\text{MgSiO}_3$  liquidus temperature of 5400 K at 140 GPa [39]. Our results for the silicate melting curve are well approximated over the relevant pressure range by the Simon-like power law [61]

$$T_{\text{rock}} = 5400 \text{ K} \left( \frac{P}{140 \text{ GPa}} \right)^{0.480}. \quad (1.9)$$

The mantles of super-earths are unlikely to be composed of pure  $\text{MgSiO}_3$ . To account for the role of possible impurities, such as additional  $\text{MgO}$  in excess of  $\text{SiO}_2$ , as in the Earth’s mantle, as well as other components such as  $\text{FeO}$ ,  $\text{CaO}$  and  $\text{Al}_2\text{O}_3$ , we estimate the solidus using the cryoscopic equation [62]

$$T = T_0(1 - \ln x_0)^{-1}, \quad (1.10)$$

where  $T$  is the melting temperature of the solution,  $T_0$  that of the pure substance,  $x_0$  is the mole fraction of the pure substance and we have assumed that the entropy of melting at high pressure is equal to the gas constant [63]. With  $x_0 = 0.79$ , we reproduce the experimentally measured solidus of an Earth-like mantle composition (4100 K at 140 GPa) [39]. A more detailed treatment of the influence of composition on silicate solidus and liquids at super-earth conditions is not justified at this point owing to lack of data.

For the melting curve of pure iron, we use the *ab initio* simulation results of Morard *et al.* [56]. We have re-fit their results to (figure 3)

$$T_{\text{Fe}} = 6500 \text{ K} \left( \frac{P}{340 \text{ GPa}} \right)^{0.515}. \quad (1.11)$$

Equation (1.11) is consistent with recent diamond anvil cell experiments [64] in addition to shock wave [54] and *ab initio* [55] results. The cores of super-earths are unlikely to be pure iron. To account for freezing point depression owing to possible impurities, such as Ni, S, O and Si, we use (equation (1.10)) with  $x_0 = 0.89$ , which produces a value of the melting point that agrees with estimates of the temperature at the boundary between Earth’s liquid outer core and solid inner core [65,66].

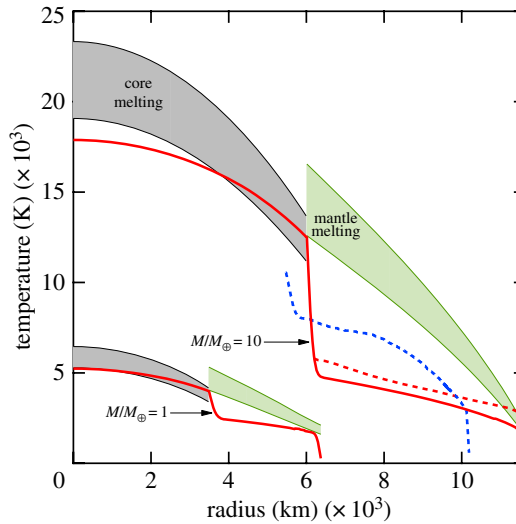


**Figure 4.** Thermal models of super-Earths: the planetary temperature (solid red), the silicate melting interval (liquid–solidus; green envelope), the core melting interval (pure iron–iron alloy) (grey envelope) compared with results of dynamical simulations: red dashed [47], blue dashed [67] ( $M/M_{\oplus} = 8$ ). (Online version in colour.)

We construct models of the temperature distribution within super-Earths by assuming that the temperature gradient is adiabatic in the interior of the mantle and the core, and that  $T_p$  and  $T_c$  are set by silicate melting (figure 4). We assume that  $T_c$  is equal to the silicate solidus at the pressure of the core–mantle boundary. We assume that  $T_p$  is also governed by silicate melting and set to a value between the solidus and liquidus temperature at the planetary surface: 1600 K, which is the value for the present-day Earth [44]. The mantle adiabat is computed from the code HeFESTo [38], whereas the core adiabat is computed from the results of *ab initio* lattice dynamics calculations [57]. We determine the variation of pressure and density with radius by solving the equations of hydrostatic equilibrium and mass conservation [15], using the HeFESTo equation of state for the mantle, assumed to be of pyrolite composition [38], and for the core, an equation of state fit to the seismologically determined properties of the Earth’s core [15].

Our thermal models produce a temperature contrast at the core–mantle boundary  $\Delta T_{\text{CMB}}$  that increases with planetary mass. Our results are approximated by

$$\Delta T_{\text{CMB}} = 1400 \text{ K} \left( \frac{M_p}{M_{\oplus}} \right)^{3/4}. \quad (1.12)$$

The mass dependence arises, because the silicate melting curve increases more rapidly with pressure than the adiabat. From equation (1.8), we have the well-known Lindemann result

$$\frac{\partial \ln T_{\text{melt}}}{\partial \ln \rho} = 2 \left( \gamma - \frac{1}{3} \right), \quad (1.13)$$

whereas for the adiabat

$$\frac{\partial \ln T_{\text{adiabat}}}{\partial \ln \rho} = \gamma \quad (1.14)$$

and the value of the Grüneisen parameter for silicates  $\gamma \sim 1$ , so that the temperature (equation (1.13)) rises more steeply on compression than equation (1.14). Our temperature profiles differ substantially from those that have been proposed before for super-Earths, particularly in the vicinity of the core–mantle boundary. For example, studies based on parametrized convection have assumed that  $\Delta T_{\text{CMB}}$  is independent of mass [15,68], and substantially smaller than the temperature contrast in the Earth. Fluid dynamical simulations of mantle convection that do not self-consistently include a core, must choose a lower boundary condition: one such study [47]

examined the case of no heating from below, implying  $\Delta T_{\text{CMB}} = 0$ , whereas van den Berg *et al.* [67] allowed for mixed heating modes and found temperatures at the core–mantle boundary for  $M_{\text{p}} = 8 M_{\oplus}$  that are not very different from what we find for  $M_{\text{p}} = 10 M_{\oplus}$ . These studies do not consider the possible effects of silicate melting on the temperature distribution and recognize  $\Delta T_{\text{CMB}}$  as one of the most uncertain parameters in thermal models of super-earths. We suggest that by considering the influence of partial melting on the thermal regulation of boundary layers, this uncertainty is reduced to that of our knowledge of material properties, including the melting curve of rock, at very high pressure.

The thermal state of super-earth cores permits magnetic field generation: a large volume of a liquid conductor is present in the form of molten iron alloy, and the freezing out of the inner core as the core cools, provides a source of latent heat and gravitational energy release for driving the field (figure 4). Super-earth cores are partially molten over the entire mass range considered. The reason for this is that silicate and iron melting temperatures are similar over the relevant pressure range (figure 3): the silicate solidus nearly coincides with the melting curve of pure iron. The tops of super-earth cores are therefore completely molten in our analysis. Because the core adiabat rises less steeply than the iron melting curve, super-earth cores cross the iron melting curve with increasing depth and are solid at their centres. Our results suggest that the size of the frozen inner core grows with planetary mass. Magnetic field generation also requires that the mantle carry heat away from the core sufficiently rapidly [69]. Combining equations (1.1) and (1.12), we find that the heat flux at the core–mantle boundary grows linearly with planetary mass

$$F_{\text{CMB}} \approx 80 \text{ mW m}^{-2} \frac{M_{\text{p}}}{M_{\oplus}}, \quad (1.15)$$

where we have scaled to an estimate of the value in the present-day Earth [70]. This heat flux must exceed the heat conducted down the adiabat for the core to convect. According to the approximate relation for the core geothermal [71], the temperature gradient at the core–mantle boundary  $\partial T / \partial r \approx -2T_{\text{c}} / R_{\text{c}} \ln(T_0 / T_{\text{c}})$ , where  $R_{\text{c}}$  is the radius of the core and  $T_0$  is the temperature at the centre. Then

$$F_{\text{cond}} \approx 2k \frac{T_{\text{c}}}{R_{\text{c}}} \ln \frac{T_0}{T_{\text{c}}} \approx 60 \text{ mW m}^{-2} \left( \frac{M_{\text{p}}}{M_{\oplus}} \right)^{1-\beta} \quad (1.16)$$

which depends weakly on planetary mass. We have assumed that  $T_{\text{c}} \propto M_{\text{p}}^{1/2}$  and that the ratio  $T_0 / T_{\text{c}}$  is independent of planetary mass in accordance with our results (figure 4). We adopt the pressure dependence of the thermal conductivity of liquid iron alloys found in a recent *ab initio* study, which yields  $k \propto M_{\text{p}}^{1/2}$ , assuming that mass scales linearly with the pressure at the core–mantle boundary [72]. Because the mass dependence of equation (1.16) is less than that of equation (1.15), the condition for core convection  $F_{\text{CMB}} > F_{\text{cond}}$  is always satisfied for super-earths, and they are expected to have dynamo-generated magnetic fields. We have assumed that  $F_{\text{CMB}}$  depends weakly on planetary mass, except through its dependence on  $\Delta T_{\text{CMB}}$ : the most important uncertainty may be in the choice of the appropriate value of  $\eta$  to use in equation (1.1), because the value of  $\eta$  may vary orders of magnitude across the boundary layer. We note that another recent study with very different approach came to similar conclusions: that long-lived magnetic fields are likely in super-earths over a wide range of masses [73].

The role of melting in influencing the thermal structure of super-earths highlights our uncertainty in material behaviour at the extreme pressure–temperature conditions that characterize the interiors of these bodies. The melting curve of silicate and iron alloys of realistic planetary composition (i.e. not pure) are still highly uncertain. For example, we have not considered here the possible consequences of incongruent melting of the  $\text{MgSiO}_3$  component at ultra-high pressure that has recently been predicted by *ab initio* simulations [74]. The viscosity of the rock component, including the influence of pressure, temperature and melt content, is another major uncertainty with an important impact on planetary cooling times: for example, *ab initio* simulations yield estimates of the diffusion coefficient, which must be scaled to the viscosity with an assumed grain size. The influence of partial melt on the viscosity is only known near ambient

pressure. The dynamics of super-earth mantles are also highly uncertain at present, with recent results arriving at very different conclusions as to the possible presence and significance of plate tectonics [75–79], and the existence of deep convection [47,48]. Our analysis suggests that future dynamical modelling efforts should consider a wider range of initial conditions, and include the influence of partial melting.

Our estimates of high-pressure material behaviour lead to the conclusion that rock–iron super-earths are likely to exhibit vigorous convection in their mantles that is sufficient to sustain dynamo-generated magnetic fields and surface volcanism. Volcanism and magnetic field generation may be important for habitability. Magnetic fields may influence habitability by protecting the planetary atmosphere against erosion by stellar winds [80]. Volcanism adds greenhouse gases to the atmosphere that may be essential for preventing or ending completely ice-covered snowball states. Some of these species also have robust spectral signatures that should be diagnostic [81]. Radio emissions [82] and co-rotational anomalies in stellar signals have been proposed as possible methods for detecting exoplanet magnetic fields. Observation of magnetic field and volcanic signatures may provide the best opportunity to constrain the thermal state of the interiors of super-earths within the habitable zone.

**Acknowledgements.** This research is supported by the European Research Council Advanced Grant ‘MoltenEarth’.

## References

1. Grasset O, Schneider J, Sotin C. 2009 A study of the accuracy of mass-radius relationships for silicate-rich and ice-rich planets up to 100 earth masses. *Astrophys. J.* **693**, 722. (doi:10.1088/0004-637X/693/1/722)
2. Charbonneau D *et al.* 2009 A super-earth transiting a nearby low-mass star. *Nature* **462**, 891–894. (doi:10.1038/nature08679)
3. Batalha NM *et al.* 2011 Kepler’s first rocky planet: Kepler-10b. *Astrophys. J.* **729**, 27. (doi:10.1088/0004-637X/729/1/27)
4. Cochran WD *et al.* 2011 KEPLER-18b, c, and d: a system of three planets confirmed by transit timing variations, light curve validation, *warm-spitzer* photometry, and radial velocity measurements. *Astrophys. J. Suppl. Ser.* **197**, 7. (doi:10.1088/0067-0049/197/1/7)
5. Lissauer JJ *et al.* 2011 A closely packed system of low-mass, low-density planets transiting Kepler-11. *Nature* **470**, 53–58. (doi:10.1038/nature09760)
6. Carter JA *et al.* 2012 Kepler-36: a pair of planets with neighboring orbits and dissimilar densities. *Science* **337**, 556–559. (doi:10.1126/science.1223269)
7. Fressin F *et al.* 2012 Two earth-sized planets orbiting Kepler-20. *Nature* **482**, 195–198. (doi:10.1038/nature10780)
8. Gillon M *et al.* 2012 Improved precision on the radius of the nearby super-Earth 55 Cnc e. *Astron. Astrophys.* **539**, A28. (doi:10.1051/0004-6361/201118309)
9. Gilliland RL *et al.* 2013 Kepler-68: three planets, one with a density between that of earth and ice giants. *Astrophys. J.* **766**, 40. (doi:10.1088/0004-637X/766/1/40)
10. Borucki WJ *et al.* 2013 Kepler-62: a five-planet system with planets of 1.4 and 1.6 Earth radii in the habitable zone. *Science* **340**, 587–590. (doi:10.1126/science.1234702)
11. Barclay T *et al.* 2013 A super-earth-sized planet orbiting in or near the habitable zone around a sun-like star. *Astrophys. J.* **768**, 101. (doi:10.1088/0004-637X/768/2/101)
12. Kite ES, Manga M, Gaidos E. 2009 Geodynamics and rate of volcanism on massive earth-like planets. *Astrophys. J.* **700**, 1732. (doi:10.1088/0004-637X/700/2/1732)
13. Gaidos E, Conrad CP, Manga M, Hernlund J. 2010 Thermodynamic limits on magnetodynamos in rocky exoplanets. *Astrophys. J.* **718**, 596. (doi:10.1088/0004-637X/718/2/596)
14. Sotin C, Labrosse S. 1999 Three-dimensional thermal convection in an iso-viscous, infinite Prandtl number fluid heated from within and from below: applications to the transfer of heat through planetary mantles. *Phys. Earth Planet. Interiors* **112**, 171–190. (doi:10.1016/S0031-9201(99)00004-7)
15. Valencia D, O’Connell RJ, Sasselov D. 2006 Internal structure of massive terrestrial planets. *Icarus* **181**, 545–554. (doi:10.1016/j.icarus.2005.11.021)

16. Demory BO, Gillon M, Seager S, Benneke B, Deming D, Jackson B. 2012 Detection of thermal emission from a super-Earth. *Astrophys. J. Lett.* **751**, L28. (doi:10.1088/2041-8205/751/2/L28)
17. Stixrude L, de Koker N, Sun N, Mookherjee M, Karki BB. 2009 Thermodynamics of silicate liquids in the deep earth. *Earth Planet. Sci. Lett.* **278**, 226–232. (doi:10.1016/j.epsl.2008.12.006)
18. van Summeren J, Conrad CP, Gaidos E. 2011 Mantle convection, plate tectonics, and volcanism on hot exo-Earths. *Astrophys. J. Lett.* **736**, L15. (doi:10.1088/2041-8205/736/1/L15)
19. Khurana KK, Jia XZ, Kivelson MG, Nimmo F, Schubert G, Russell CT. 2011 Evidence of a global magma ocean in Io's interior. *Science* **332**, 1186–1189. (doi:10.1126/science.1201425)
20. McWilliams RS, Spaulding DK, Eggert JH, Celliers PM, Hicks DG, Smith RF, Collins GW, Jeanloz R. 2012 Phase transformations and metallization of magnesium oxide at high pressure and temperature. *Science* **338**, 1330–1333. (doi:10.1126/science.1229450)
21. Kaula WM. 1979 Thermal evolution of Earth and Moon growing by planetesimal impacts. *J. Geophys. Res.* **84**, 999–1008. (doi:10.1029/JB084iB03p00999)
22. Pierazzo E, Vickery AM, Melosh HJ. 1997 A reevaluation of impact melt production. *Icarus* **127**, 408–423. (doi:10.1006/icar.1997.5713)
23. Solomatov VS, Stevenson DJ. 1993 Nonfractional crystallization of a terrestrial magma ocean. *J. Geophys. Res. Planets* **98**, 5391–5406. (doi:10.1029/92JE02579)
24. Tonks WB, Melosh HJ. 1993 Magma ocean formation due to giant impacts. *J. Geophys. Res. Planets* **98**, 5319–5333. (doi:10.1029/92JE02726)
25. Pavani R, Ranghino G. 1982 A method to compute the volume of a molecule. *Comput. Chem.* **6**, 133–135. (doi:10.1016/0097-8485(82)80006-5)
26. Canup RM. 2012 Forming a moon with an Earth-like composition via a giant impact. *Science* **338**, 1052–1055. (doi:10.1126/science.1226073)
27. Watters WA, Zuber MT, Hager BH. 2009 Thermal perturbations caused by large impacts and consequences for mantle convection. *J. Geophys. Res. Planets* **114**, E02001.
28. Kraus RG *et al.* 2012 Shock vaporization of silica and the thermodynamics of planetary impact events. *J. Geophys. Res. Planets* **117**, E09009.
29. Flasar FM, Birch F. 1973 Energetics of core formation: a correction. *J. Geophys. Res.* **78**, 6101–6103. (doi:10.1029/JB078i026p06101)
30. Samuel H, Tackley PJ, Evonuk M. 2010 Heat partitioning in terrestrial planets during core formation by negative diapirism. *Earth Planet. Sci. Lett.* **290**, 13–19. (doi:10.1016/j.epsl.2009.11.050)
31. Ricard Y, Sramek O, Dubuffet F. 2009 A multi-phase model of runaway core–mantle segregation in planetary embryos. *Earth Planet. Sci. Lett.* **284**, 144–150. (doi:10.1016/j.epsl.2009.04.021)
32. Ghosh A, McSween HY. 1998 A thermal model for the differentiation of asteroid 4 vesta, based on radiogenic heating. *Icarus* **134**, 187–206. (doi:10.1006/icar.1998.5956)
33. Tang HL, Dauphas N. 2012 Abundance, distribution, and origin of <sup>60</sup>Fe in the solar protoplanetary disk. *Earth Planet. Sci. Lett.* **359**, 248–263. (doi:10.1016/j.epsl.2012.10.011)
34. Ammann MW, Brodholt JP, Wookey J, Dobson DP. 2010 First-principles constraints on diffusion in lower-mantle minerals and a weak D'' layer. *Nature* **465**, 462–465. (doi:10.1038/nature09052)
35. Karki BB, Stixrude LP. 2010 Viscosity of MgSiO<sub>3</sub> liquid at Earth's mantle conditions: implications for an early magma ocean. *Science* **328**, 740–742. (doi:10.1126/science.1188327)
36. Mei S, Bai W, Hiraga T, Kohlstedt DL. 2002 Influence of melt on the creep behavior of olivine-basalt aggregates under hydrous conditions. *Earth Planet. Sci. Lett.* **201**, 491–507. (doi:10.1016/S0012-821X(02)00745-8)
37. Lejeune AM, Richet P. 1995 Rheology of crystal-bearing silicate melts: an experimental study at high viscosities. *J. Geophys. Res. Solid Earth* **100**, 4215–4229. (doi:10.1029/94JB02985)
38. Stixrude L, Lithgow-Bertelloni C. 2011 Thermodynamics of mantle minerals. II. Phase equilibria. *Geophys. J. Int.* **184**, 1180–1213. (doi:10.1111/j.1365-246X.2010.04890.x)
39. Fiquet G, Auzende AL, Siebert J, Corgne A, Bureau H, Ozawa H, Garbarino G. 2010 Melting of peridotite to 140 gigapascals. *Science* **329**, 1516–1518. (doi:10.1126/science.1192448)
40. O'Brien DP, Morbidelli A, Levison HF. 2006 Terrestrial planet formation with strong dynamical friction. *Icarus* **184**, 39–58. (doi:10.1016/j.icarus.2006.04.005)
41. Ida S, Lin DNC. 2010 Toward a deterministic model of planetary formation. VI. Dynamical interaction and coagulation of multiple rocky embryos and super-earth systems around solar-type stars. *Astrophys. J.* **719**, 810. (doi:10.1088/0004-637X/719/1/810)

42. Pollack HN, Hurter SJ, Johnson JR. 1993 Heat flow from the Earth's interior: analysis of the global data set. *Rev. Geophys.* **31**, 267–280. (doi:10.1029/93RG01249)
43. Mitrovica JX. 1996 Haskell [1935] revisited. *J. Geophys. Res. Solid Earth* **101**, 555–569. (doi:10.1029/95JB03208)
44. Hirschmann MM. 2006 Water, melting, and the deep Earth H<sub>2</sub>O cycle. *Annu. Rev. Earth Planet. Sci.* **34**, 629–653. (doi:10.1146/annurev.earth.34.031405.125211)
45. Labrosse S, Hernlund JW, Coltice N. 2007 A crystallizing dense magma ocean at the base of the Earth's mantle. *Nature* **450**, 866–869. (doi:10.1038/nature06355)
46. Tozer DC. 1972 The present thermal state of the terrestrial planets. *Phys. Earth Planet. Interiors* **6**, 182–197. (doi:10.1016/0031-9201(72)90052-0)
47. Tackley PJ, Ammann M, Brodholt JP, Dobson DP, Valencia D. 2013 Mantle dynamics in super-Earths: post-perovskite rheology and self-regulation of viscosity. *Icarus* **225**, 50–61. (doi:10.1016/j.icarus.2013.03.013)
48. Stamenkovic V, Noack L, Breuer D, Spohn T. 2012 The influence of pressure-dependent viscosity on the thermal evolution of super-earths. *Astrophys. J.* **748**, 41. (doi:10.1088/0004-637X/748/1/41)
49. Williams Q, Garnero EJ. 1996 Seismic evidence for partial melt at the base of Earth's mantle. *Science* **273**, 1528–1530. (doi:10.1126/science.273.5281.1528)
50. Stixrude L, Karki B. 2005 Structure and freezing of MgSiO<sub>3</sub> liquid in Earth's lower mantle. *Science* **310**, 297–299. (doi:10.1126/science.1116952)
51. Akins JA, Luo SN, Asimow PD, Ahrens TJ. 2004 Shock-induced melting of MgSiO<sub>3</sub> perovskite and implications for melts in Earth's lowermost mantle. *Geophys. Res. Lett.* **31**, L14612. (doi:10.1029/2004GL020237)
52. Holland KG, Ahrens TJ. 1997 Melting of (Mg,Fe)<sub>2</sub>SiO<sub>4</sub> at the core–mantle boundary of the earth. *Science* **275**, 1623–1625. (doi:10.1126/science.275.5306.1623)
53. Spaulding DK, McWilliams RS, Jeanloz R, Eggert JH, Celliers PM, Hicks DG, Collins GW, Smith RF. 2012 Evidence for a phase transition in silicate melt at extreme pressure and temperature condition. *Phys. Rev. Lett.* **108**, 065701. (doi:10.1103/PhysRevLett.108.065701)
54. Brown JM, McQueen RG. 1986 Phase transitions, Grüneisen parameter, and elasticity for shocked iron between 77 GPa and 400 GPa. *J. Geophys. Res.* **91**, 7485–7494. (doi:10.1029/JB091iB07p07485)
55. Alfè D, Price GD, Gillan MJ. 2002 Iron under Earth's core conditions: liquid-state thermodynamics and high-pressure melting curve from *ab initio* calculations. *Phys. Rev. B* **65**, 165118. (doi:10.1103/PhysRevB.65.165118)
56. Morard G, Bouchet J, Valencia D, Mazevet S, Guyot F. 2011 The melting curve of iron at extreme pressures: implications for planetary cores. *High Energy Density Phys.* **7**, 141–144. (doi:10.1016/j.hedp.2011.02.001)
57. Stixrude L. 2012 Structure of iron to 1 Gbar and 40 000 K. *Phys. Rev. Lett.* **108**, 055505. (doi:10.1103/PhysRevLett.108.055505)
58. Wolf GH, Jeanloz R. 1984 Lindemann melting law: anharmonic correction and test of its validity for minerals. *J. Geophys. Res.* **89**, 7821–7835. (doi:10.1029/JB089iB09p07821)
59. Murakami M, Hirose K, Kawamura K, Sata N, Ohishi Y. 2004 Post-perovskite phase transition in MgSiO<sub>3</sub>. *Science* **304**, 855–858. (doi:10.1126/science.1095932)
60. Umemoto K, Wentzcovitch RM, Allen PB. 2006 Dissociation of MgSiO<sub>3</sub> in the cores of gas giants and terrestrial exoplanets. *Science* **311**, 983–986. (doi:10.1126/science.1120865)
61. Ross M. 1969 Generalized Lindemann melting law. *Phys. Rev.* **184**, 233–242. (doi:10.1103/PhysRev.184.233)
62. Atkins PW. 1994 *Physical chemistry*, 5th edn. New York, NY: Freeman.
63. Stishov SM, Makarenko IN, Ivanov VA, Nikolaenko AM. 1973 On the entropy of melting. *Phys. Lett. A* **45**, 18. (doi:10.1016/0375-9601(73)90485-4)
64. Anzellini S, Dewaele A, Mezouar M, Loubeyre P, Morard G. 2013 Melting of iron at Earth's inner core boundary based on fast X-ray diffraction. *Science* **340**, 464–466. (doi:10.1126/science.1233514)
65. Steinle-Neumann G, Stixrude L, Cohen RE. 2002 Physical properties of iron in the inner core. In *Core structure, dynamics, and rotation* (eds V Dehant, K Creager, S Zatman, S-I Karato), pp. 137–161. Washington, DC: American Geophysical Union.
66. Alfè D, Gillan MJ, Price GD. 2002 Composition and temperature of the Earth's core constrained by combining *ab initio* calculations and seismic data. *Earth Planet. Sci. Lett.* **195**, 91–98. (doi:10.1016/S0012-821X(01)00568-4)

67. van den Berg AP, Yuen DA, Beebe GL, Christiansen MD. 2010 The dynamical impact of electronic thermal conductivity on deep mantle convection of exosolar planets. *Phys. Earth Planet. Inter.* **178**, 136–154. (doi:10.1016/j.pepi.2009.11.001)
68. Sotin C, Grasset O, Mocquet A. 2007 Mass-radius curve for extrasolar Earth-like planets and ocean planets. *Icarus* **191**, 337–351. (doi:10.1016/j.icarus.2007.04.006)
69. Nimmo F, Price GD, Brodholt J, Gubbins D. 2004 The influence of potassium on core and geodynamo evolution. *Geophys. J. Int.* **156**, 363–376. (doi:10.1111/j.1365-246X.2003.02157.x)
70. Lay T, Hernlund J, Buffett BA. 2008 Core–mantle boundary heat flow. *Nat. Geosci.* **1**, 25–32. (doi:10.1038/ngeo.2007.44)
71. Labrosse S. 2003 Thermal and magnetic evolution of the Earth's core. *Phys. Earth Planet. Inter.* **140**, 127–143. (doi:10.1016/j.pepi.2003.07.006)
72. Pozzo M, Davies C, Gubbins D, Alfè D. 2012 Thermal and electrical conductivity of iron at Earth's core conditions. *Nature* **485**, 355–358. (doi:10.1038/nature11031)
73. Tachinami C, Senshu H, Ida S. 2011 Thermal evolution and lifetime of intrinsic magnetic fields of super-earths in habitable zones. *Astrophys. J.* **726**, 70. (doi:10.1088/0004-637X/726/2/70)
74. Boates B, Bonev SA. 2013 Demixing instability in dense molten MgSiO<sub>3</sub> and the phase diagram of MgO. *Phys. Rev. Lett.* **110**, 135504. (doi:10.1103/PhysRevLett.110.135504)
75. Valencia D, O'Connell RJ, Sasselov DD. 2007 Inevitability of plate tectonics on super-earths. *Astrophys. J.* **670**, L45. (doi:10.1086/524012)
76. O'Neill C, Lenardic A. 2007 Geological consequences of super-sized earths. *Geophys. Res. Lett.* **34**, L19204. (doi:10.1029/2007GL030598)
77. van Heck HJ, Tackley PJ. 2011 Plate tectonics on super-Earths: equally or more likely than on earth. *Earth Planet. Sci. Lett.* **310**, 252–261. (doi:10.1016/j.epsl.2011.07.029)
78. Korenaga J. 2010 On the likelihood of plate tectonics on super-Earths: does size matter? *Astrophys. J. Lett.* **725**, L43. (doi:10.1088/2041-8205/725/1/L43)
79. Foley BJ, Bercovici D, Landuyt W. 2012 The conditions for plate tectonics on super-Earths: inferences from convection models with damage. *Earth Planet. Sci. Lett.* **331**, 281–290. (doi:10.1016/j.epsl.2012.03.028)
80. Dehant V *et al.* 2007 Planetary magnetic dynamo effect on atmospheric protection of early Earth and Mars. *Space Sci. Rev.* **129**, 279–300. (doi:10.1007/s11214-007-9163-9)
81. Tinetti G *et al.* 2012 EChO. *Exp. Astron.* **34**, 311–353. (doi:10.1007/s10686-012-9303-4)
82. Driscoll P, Olson P. 2011 Optimal dynamos in the cores of terrestrial exoplanets: magnetic field generation and detectability. *Icarus* **213**, 12–23. (doi:10.1016/j.icarus.2011.02.010)